© 2019. Published by The Company of Biologists Ltd | Development (2019) 146, dev176933. doi:10.1242/dev.176933

RESEARCH ARTICLE

Dynamic Hh signalling can generate temporal information during tissue patterning

Diana García-Morales[1], Tomás Navarro[1], Antonella Iannini[1], Paulo S. Pereira[2], David G. Míguez[3,*] and Fernando Casares[1,*]

ABSTRACT

The differentiation of tissues and organs requires that cells exchange information in space and time. Spatial information is often conveyed by morphogens: molecules that disperse across receiving cells to generate signalling gradients. Cells translate such concentration gradients into space-dependent patterns of gene expression and cellular behaviour. But could morphogen gradients also convey developmental time? Here, by investigating the developmental role of Hh on a component of the *Drosophila* visual system, the ocellar retina, we have discovered that ocellar cells use the non-linear gradient of Hh as a temporal cue, collectively performing the biological equivalent of a mathematical logarithmic transformation. In this way, a morphogen diffusing from a non-moving source is decoded as a wave of differentiating photoreceptors that travels at constant speed throughout the retinal epithelium.

KEY WORDS: *Drosophila*, Hedgehog, Patterning, Systems modelling, Visual system

INTRODUCTION

Morphogens of the *hedgehog* (*hh*)/Shh family contribute spatial information during the development of a wide range of organs and organisms (Ingham et al., 2011; Briscoe and Thérond, 2013). Produced at specialized sites within developing organs, Hh molecules disperse and receiving cells respond according to the Hh concentration that reaches them. The mechanisms of Hh dispersion are not yet fully understood, and include potential transport in exovesicles or associated with specialized filopodia, called cytonemes. The lipid modifications of Hh (by cholesterol and palmitic acid) tether it to the membrane, ruling out free diffusion as the major transport mechanism for Hh (reviewed by Simon et al., 2016). In receiving cells, Hh molecules bind to membrane receptors of the *patched* (*ptc*) family. In *Drosophila,* the receptor Ptc (Nakano et al., 1989) forms a receptor complex that also includes the adhesion molecules iHog and Boi (Bilioni et al., 2013). Hh binding to Ptc relieves the repression of Smoothened (Smo) by Ptc, which, in turn, blocks the processing of the Gli transcription factor *cubitus interruptus* (Ci) into its repressor form. The result of this double-negative regulation is the stabilization and activation of full-length Ci (CiA), which then acts as a transcriptional activator of Hh pathway targets (Aza-Blanc et al., 1997; Alexandre et al., 1996). One of the target genes activated by Hh is the receptor *ptc* itself (Hidalgo and Ingham, 1990; Capdevila et al., 1994). Because Ptc is simultaneously the Hh receptor and a positive target of the pathway, it plays a very important dynamic role in Hh-driven patterning processes. As the pathway is activated, Ptc expression rises closest to the source (where higher Hh levels are received), trapping increasing amounts of Hh. This mechanism allows the reshaping of the Hh gradient as time passes, starting from shallower longer-reaching gradients to steeper shorter-reaching ones. This phenomenon has been observed both in *Drosophila* and vertebrate systems, and is important in establishing dynamically different domains of gene expression at different distances from the Hh source (Gallet and Therond, 2005; Nahmad and Stathopoulos, 2009; Dessaud et al., 2007; Chamberlain et al., 2008).

However, and although Hh signalling has been mostly involved in spatial patterning, in two systems Hh has also been shown to be required for temporal patterning – i.e. the reiteration of a developmental process at a particular pace. During the development of the *Drosophila* compound eye, Hh drives a wave of photoreceptor (R) cell differentiation across the eye primordium at a constant speed (Ma et al., 1993; Heberlein et al., 1993). A similar Shh moving wave has been described during the differentiation of the ganglion cells in the zebrafish retina (Neumann and Nuesslein-Volhard, 2000). However, these waves are not generated based on the morphogen characteristics of Hh/Shh (i.e. differential responses to varying Hh concentration in space), but on the fact that the source of Hh production itself moves across the developing retina: Hh/Shh molecules are expressed in differentiating retinal cells (R cells in *Drosophila* and ganglion cells in zebrafish) and non-autonomously induce progenitors to differentiate into retina cells that, in turn, start producing Hh/Shh. In this way, the source of signalling molecule moves coupled to the differentiation process.

In *Drosophila,* the compound eye develops from the cephalic disc (also called the 'eye-antennal' disc), a monolayered epithelial sac that additionally gives rise to another component of the fly visual system: the ocellar complex. This complex comprises three small camera-type eyes, or *ocelli* (one anterior ocellus and two posterior ocelli), located on the forehead of the fly that are part of the visual system of most insects (Fig. 1A,B). Similar to the compound eye, the specification of the ocelli requires Hh signalling (Royet and Finkelstein, 1996; Blanco et al., 2009; Aguilar-Hidalgo et al., 2013). In the prospective ocellar complex region of the disc, one domain of Hh expression is flanked by two regions competent to differentiate into the ocellar photoreceptors (R cells) under the action of Hh signalling. One marker of competence is the gene *eyes absent* (*eya*) (Blanco et al., 2009; Aguilar-Hidalgo et al., 2013) (Fig. 1C,D). When the two contralateral discs fuse, the anterior ocellar regions merge into the single anterior ocellus (aOC), while the two other regions remain separate and will develop into the paired posterior ocelli (pOC). Previous work has defined the gene

[1]CABD (CSIC-Universidad Pablo de Olavide-Junta de Andalucía), GEM-DMC2 Unit, Campus UPO, 41013 Seville, Spain. [2]Instituto de Biologia Molecular e Celular/i3S, Universidade do Porto, 4200-135 Porto, Portugal. [3]Centro de Biología Molecular Severo Ochoa (CSIC-UAM), Campus de Cantoblanco, 28049 Madrid, Spain.

*Authors for correspondence (fcasfer@upo.es; david.miguez@uam.es)

F.C., 0000-0002-2181-3858

Received 14 February 2019; Accepted 19 March 2019

Development (2019) 146, dev176933. doi:10.1242/dev.176933

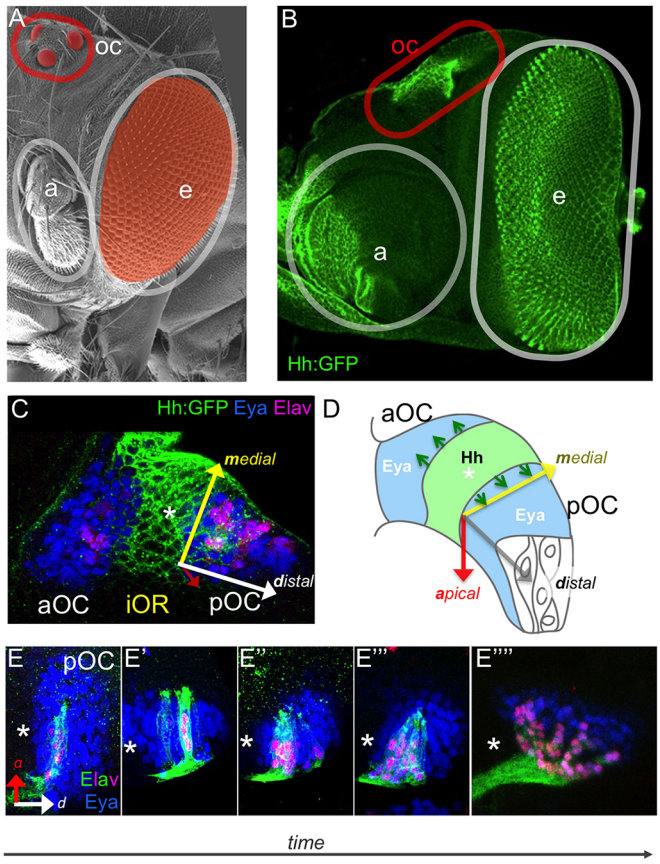

Fig. 1. Photoreceptor (R) differentiation in the *Drosophila* ocelli. (A) Scanning electron microscope view of a *Drosophila* head. The ocelli (oc), the compound eye (ce) (both pseudocoloured) and the antenna (a) are outlined. (B) Confocal image of an eye-antennal head primordium of a Hh:GFP-BAC larva (late third instar) marking the prospective ocelli, compound eye and antenna. Hh:GFP is in green. (C) Higher-magnification of the prospective ocellar region of a Hh:GFP-BAC primordium (green) stained for Eya (competence marker, blue) and Elav (neural marker, magenta). Hh is produced from a central domain that will become the interocellar region (iOR). The position of the Hh-expressing domain is marked with and asterisk in C-E''''. Adjacent to it, the anterior and posterior domains of Eya-expressing cells will become the anterior (aOC) and posterior (pOC) ocelli, respectively. (D) Schematic representation of the ocellar region, showing the Hh-producing and Eya-expressing domains. The arrows indicate the spatial axes. (E-E'''') Temporal series of pOC regions from progressively older larvae/early pupa (as indicated by the 'time' arrow), marked with Eya (blue) and Elav (Elav>nRFP_ires_mGFP). Images are from different, fixed discs. Elav-expressing photoreceptor ('R') cells appear first closest to the Hh source (E) and then accumulate successively in more distal regions (E'-E''''). Nuclei and membranes of Elav cells are marked in magenta and green, respectively.

regulatory network that, under the control of Hh, results in the specification of the OC competent regions and regulates their size (Aguilar-Hidalgo et al., 2013, 2016). Here, we further investigate the role of Hh in the next developmental step: the differentiation of the ocellar retinas. First we find that, in the ocelli, R differentiation also proceeds as a wave of constant speed, and that this wave depends on Hh. However, and in contrast to the compound eye, Hh is not expressed in ocellar R cells, but remains expressed in a spatially static source. Our work further shows how the non-linear gradient that emanates from this source of Hh signal can in principle be translated into a wave of R differentiation with constant speed, owing to a single modification in the Hh signalling pathway: the attenuation of Ptc expression as R cells differentiate. Thus, Hh, produced at a spatially static source, can be read as a 'time arrow' during R differentiation.

RESULTS AND DISCUSSION

In order to study how Hh signalling controls the differentiation of the ocellar retinas, we first set to study the dynamics of R cell differentiation, focusing on the larger posterior ocellus.

The ocellar competent regions, which abut the Hh-expressing domain, can be labelled with Eya, and R differentiation can be followed using the neuronal markers Elav and Glass. In fixed discs of increasing age, we observed that R cell differentiation proceeded in a wave-like fashion – i.e. differentiation starts in the vicinity of the Hh source and then progress in a proximal-distal direction across the ocellar tissue (Fig. 1E). The transition from precursors to R cells can be monitored using the precursor marker gene *senseless* (*sens*) (Nolo et al., 2000) (Fig. 1, Fig. S1A-C). We find that, as in the compound eye, Sens expression precedes temporally that of Elav. Sens expression in differentiating R cells is transient, and it decreases as Elav expression increases. Spatially, Sens and Elav distribute along a proximal-distal axis with respect to the Hh source. Therefore, the differentiation wave can be visualized as a succession of Elav and Sens along this axis, with new Sens-expressing cells being added progressively further away from the Hh source as differentiating cells express Elav and downregulate Sens (Fig. 1, Fig. S1). Importantly, and in contrast to the moving wave of Hh that sweeps across the developing compound eye, Hh is never expressed in ocellar R cells (Fig. 1, Fig. S1D,D′) (Aguilar-Hidalgo et al., 2013; Amin et al., 1999). The Hh source remains the inter-ocellar region and, therefore, does not move in space. To start investigating the potential role of Hh signalling in organizing this wave, we first examined the distribution of Hh across the competence domain, which is about 40 µm (10 cells) wide, using a Hh:GFP BAC construct (Chen et al., 2017). Hh:GFP disperses away from its source following roughly a decaying exponential (Fig. 2A,A′ and see below). The Hh receptor Patched (Ptc) is also a target of the signalling pathway, so that its expression can be used as a read-out of the signalling activity of the pathway (Nakano et al., 1989). We found that, before R differentiation starts, Ptc expression follows the Hh:GFP gradient (Fig. 2A,A′ and see below), indicating that Ptc signalling intensity reflects Hh distribution across the ocellus. In addition, this result suggested that the non-uniform Hh distribution could contribute to generating the wave, transforming the spatial gradient into a temporal axis, such that cells closer to the Hh source (and therefore receiving a higher concentration of Hh) would differentiate earlier than cells farther away. To test this possibility, we equalized Hh signalling across the developing ocellus by expressing, specifically in the ocellar primordia, uniform levels of *cubitus interuptus* (*ci*), the Gli-type nuclear transducer of the Hh pathway (Fig. 2B,C, Fig. S2A,B). As the stabilization of Ci depends on Hh signalling (and this signalling decays as the distance from the source increases), we drove expression of a mutant form of Ci that cannot be phosphorylated by PKA ('Ci-PKA') and, hence, is not cleaved into the repressive form of Ci (Methot and Basler, 2000). In *eyaL>Ci-PKA* ocelli, a larger than normal number of cells had initiated the expression of Sens and Elav relative to control ocelli, indicating their premature differentiation. More importantly, the progression of the wave seemed disrupted: instead of the succession of Elav and Sens cells, Elav and Sens cells are intermingled in Ci-overexpressing ocelli (Fig. 2B,C). This result was compatible with the idea that the Hh signalling gradient encodes a temporal axis that generates the wave-like differentiation of ocellar R cells. To test this point more directly, we distorted the normal distribution of Hh by

Development (2019) 146, dev176933. doi:10.1242/dev.176933

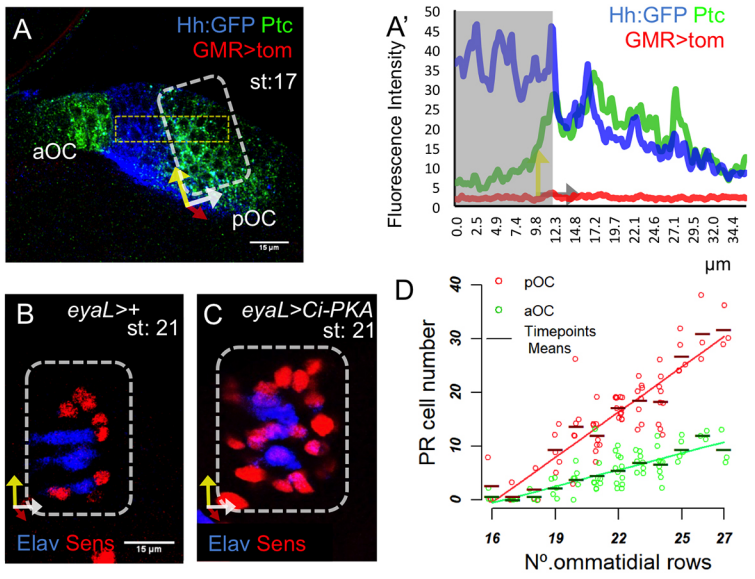

Fig. 2. Hh signalling and R differentiation wave. (A) Confocal image of the ocellar region of a Hh:GFP; GMR>tdTomato ('GMR>tom') larva (stage 17 ommatidia), stained for Hh:GFP (blue), Ptc (green) and anti-Tomato (red). No R cells ('GMR>tom') have as yet differentiated. (A′) Quantitative profiles of the Hh:GFP, Ptc and GMR signals across the Hh-producing domain (shaded in grey) and the pOC (measured in the dashed yellow box in A). Hh:GFP signal decays non-linearly. Ptc signal follows that of Hh:GFP at this stage, when no R cell (GMR>Tom) has yet differentiated. (B,C) pOC regions (boxed, like the corresponding region in A) stained for Elav (blue) and Sens (red) of discs from larvae of the same stage (21 ommatidia). In the control (B, 'eyaL>+') a row of R-expressing Elav cells precedes a row of Sens-expressing precursors. In eyaL>Ci-PKA (C, causing the uniform expression of Ci), precocious differentiation is observed. In addition, the differentiation wave, characterized by the succession Elav→Sens, is broken. (D) Number of Elav-positive cells in the pOC (red) and aOC (green) as a function of developmental time. The number of ommatidial rows in the compound eye, which increases linearly with time, was used as an internal developmental timer. Individual data points (circles) and the means are represented and fit well to a line. See Materials and Methods for a description of the statistical analysis.

inducing new foci of Hh expression from around the developing ocelli (*wg2.11*-GAL4; *UAS-GFP:Hh* or '*wg>Hh*'; Pereira et al., 2006 and Fig. 3) to then compared the spatial patterns of Elav^{+}Sens^{-}, Elav^{+}Sens^{+} and Elav^{-}Sens^{+} cells between control and *wg>Hh* ocelli (Fig. 3A-D′). Because even the wild-type pattern shows some variability, we used a statistical analysis to compare the 'grouping' (as measured by the departure from a random proportion of neighbours of a given type) and 'polarity', which measures the ordered succession of cell states along the proximodistal axis (and is a defining trait of a wave) (Fig. S3A-C′). Control and *wg>Hh* patterns were both significantly – but similarly – different from random (Fig. S3D), as expected if spatially localized Hh drives the pattern of differentiation. However, when 'polarity', the metrics that reflects a wave-like organization, was analysed, control samples were significantly more polarized than *wg>Hh*, which were closer to a non-polarized distribution (Fig. S3E; see Materials and Methods for a complete description of the statistical analysis). We subjected the ocellar patterns of *eyaL>Ci-PKA* larvae to the same analysis and found also that they were close to non-polarized (Fig. S3E). These results confirm that, despite the variability of the system, the pattern of differentiation from Sens precursors to Elav photoreceptors progresses as a wave, and reinforce the notion that the distribution of Hh across the developing ocellus is necessary for organizing this wave.

Next, we tested whether blocking Hh signalling could result in abrogation of R differentiation. To do that, we expressed a dominant-negative Ptc receptor (PtcΔloop2), which, due to its incapacity to bind Hh, represses the pathway constitutively (Briscoe et al., 2001). Our results show that, as in the compound eye, Hh is necessary for R differentiation in the ocelli (Fig. S2C-E). Altogether, our results so far indicated that the time needed for a cell to start differentiating depends on the amount of Hh that it receives.

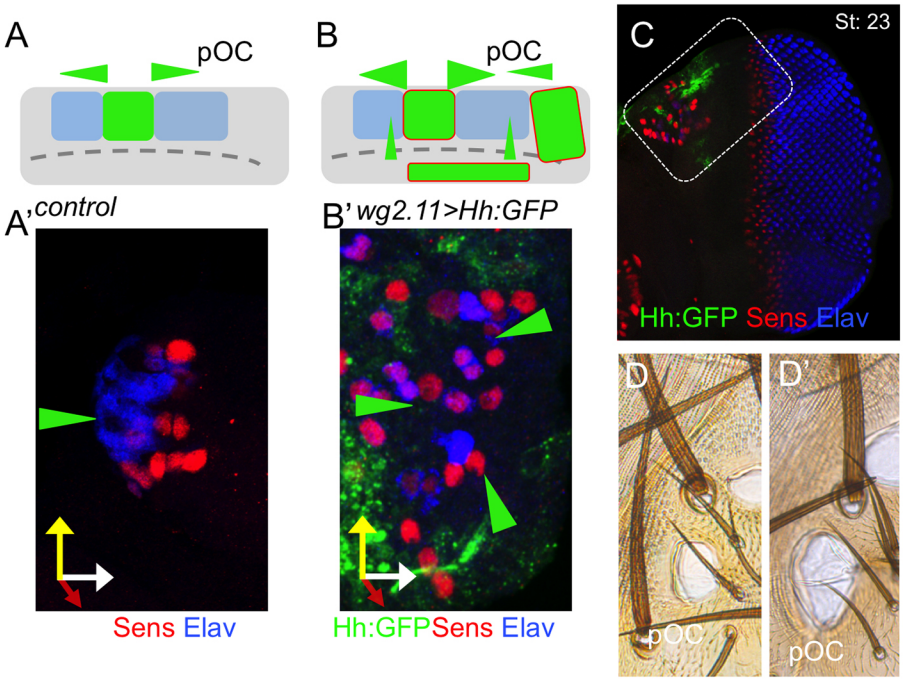

Fig. 3. Altering Hh spatial distribution distorts the differentiation wave. (A,B) Cartoon depiction of the Hh sources (green domains) relative to the retina-competent regions (blue) in control (A) and *wg>Hh* (B) ocellar regions. The posterior ocellus is marked as 'pOC'. The green triangles indicate the distribution of Hh from these sources. In *wg>Hh,* Hh is expressed around the ocelli and within the normal Hh expression domain. (C) Late *wg>Hh* disc (stage 23) stained for GFP (GFP:Hh), Sens and Elav. The boxed region corresponds to that represented in A and B. A′ and B′ are pOC regions from control and *wg>Hh* individuals, respectively. (D,D′) Ocelli of control (D) and *wg>Hh* (D′) adults. In *wg>Hh*, ocelli are larger.

Development (2019) 146, dev176933. doi:10.1242/dev.176933

Because Hh distribution decays non-linearly in space (Fig. 2A′), R cells should also accumulate non-linearly over time (i.e. with fast R cell generation close to the source and progressively slowing down with increasing distance from it). To test this hypothesis, we quantified the number of Elav-expressing R cells over developmental time. As developmental timer, we used the number of rows of ommatidia that have undergone differentiation in the compound eye, which is known to increase at a constant speed (Wartlick et al., 2014; Vollmer et al., 2016) at least during the second half of the last larval stage (Spratford and Kumar, 2013), the period during which ocellar differentiation takes place. In contrast with the expectation, though, the number of Elav cells increased linearly with time in both anterior and posterior ocelli, indicating that the differentiation wave propagated at a constant speed (Fig. 2D).

In order to explore the signalling outputs in this system, we constructed a mathematical model capturing the essence of the Hh signalling pathway (see Materials and Methods). In this model, Ptc represses Hh signalling targets unless it binds Hh. As Ptc is one of the targets of the pathway, Hh binding to Ptc releases the repressive action of Ptc and results in its upregulation (Nakano et al., 1989). Sens is included as a target in the model, although this does not imply that Sens is a direct target. Expression of Elav in Sens-expressing precursors follows irreversibly, and to reflect the loss of Sens expression observed in Elav cells, we have also included a negative feedback from Elav to Sens (see Fig. 4A). The dynamics of Hh production and dispersion in the model were calibrated using measured Hh:GFP profiles determined experimentally (Fig. S4; and see Table S1 for values, units and source of parameters). The intrinsic variability of the system is modelled by introducing a 20% variability in all parameters of the model (see Materials and Methods). In brief, the model simulates a two-dimensional array of 10×10 cells (see Fig. S5 and Movies 1 and 2) that respond to an external concentration of Hh. Hh is being secreted at one of boundaries of the system and diffuses through the array. The response to Hh in each cell is simulated by numerically solving a set of ordinary differential equations (ODEs) that model a simplified version of the Hh signalling pathway (Fig. 4A, see Materials and Methods). With no further assumptions, the model simulations confirmed the prior expectation: the accumulation of Elav cells was non-linear and differentiation was often not completed during the developmental period allowed (40 h) (Fig. 4B). The fact that the model was unable to reproduce the experimental observations indicated that our understanding of the signalling dynamics was missing some important process. Owing to the key relevance of Ptc as both Hh receptor and target of the pathway, we examined in detail the dynamics of Ptc accumulation during differentiation. We found that, although before R cell differentiation Ptc signal followed a non-linear decay with a strong peak close to the Hh source (see Fig. 2A,A′), at later stages Ptc signal decreased dramatically in R cells, identified by expression of Elav (Fig. 4C-D′). As binding of Hh to Ptc reduces its mobility (Chen and Struhl, 1996), we reasoned that the reduction of Ptc availability in R cells could allow the non-bound Hh to move over these cells and disperse farther away from the source. In this model, the sequential dampening of Ptc expression acts as a 'desensitization' mechanism. When this Ptc dampening was incorporated in the model (simplified as a repressor link from Elav-R to Ptc) it now correctly predicted that the differentiation wave moves with about constant velocity, and achieves the full differentiation of the progenitor population during the differentiation window (Fig. 4E) (see also Movies 1 and 2). In addition, the simulated dynamic profile of Hh matched that measured experimentally (Fig. S4), with its gradient flattening and reaching further as developmental time progresses.

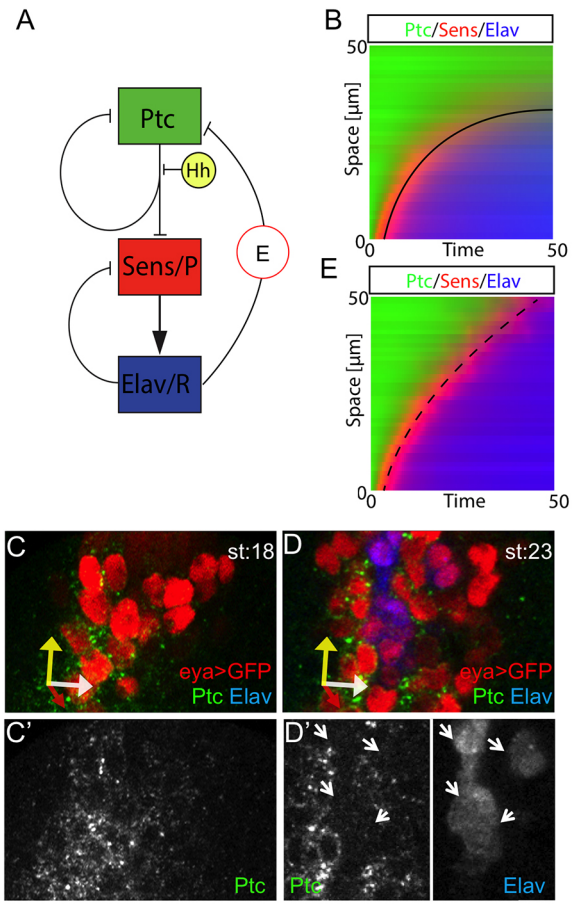

Fig. 4. Loss of Ptc in R cells suffices to explain linear differentiation dynamics. (A) Cartoon diagram of the model for the Hh signalling pathway and its downstream effects. (B,E) Spatio-temporal dynamics of the outputs of the model without considering (B) or considering (E) a negative feedback from Elav-expressing R cells to Ptc ('E' link in A). (B) R cells (blue) accumulate hyperbolically and do not reach the end of the competent region within the time frame of 50 h. (E) With negative feedback (all other parameters are the same), R accumulation dynamics are close to linear and R differentiation reaches the end of the competent region. Simulations have been carried out, including a 50% reduction in Hh production rate along the 50 h time, as observed experimentally. Similar results are obtained if this rate is constant (Fig. S5). (C,D) Ocellar region of stage 18 (C,C′) and stage 23 (D,D′) *eyaL>GFP* discs stained for GFP (marking the Eya-expressing competence domain), Ptc and Elav (R cells). Axes are as in Fig. 1. Elav-expressing cells (marked by arrows) show reduced levels of Ptc. Source code is available in the supplementary material under source code File 1.

Simulations include the ∼50% reduction of Hh:GFP production that we observed experimentally (Fig. S4A) but the results remain the same if the Hh production rate is constant (Fig. S5). Therefore, the desensitization of differentiating cells to Hh, caused by the dampening of Ptc, would allow the field of ocellar competent cells to transform the Hh gradient into a moving signalling and differentiation wave of constant speed. It has been described that Ptc is downregulated upon binding to Hh (Gallet and Therond, 2005; Incardona et al., 2002; Torroja et al., 2004) and also in a self-regulated manner (Casali, 2010) in *Drosophila* wing discs. To test whether the dramatic downregulation of Ptc we observed was due to R cell differentiation or merely to a process depending on ligand binding or Ptc concentration, we examined Ptc levels in the ocelli of late discs from *atonal* (*ato*) mutant larvae, in which R differentiation is abrogated (Fig. S6). For each disc, the levels of Ptc signal in the ocelli were normalized relative to the signal in the antenna of the

Development (2019) 146, dev176933. doi:10.1242/dev.176933

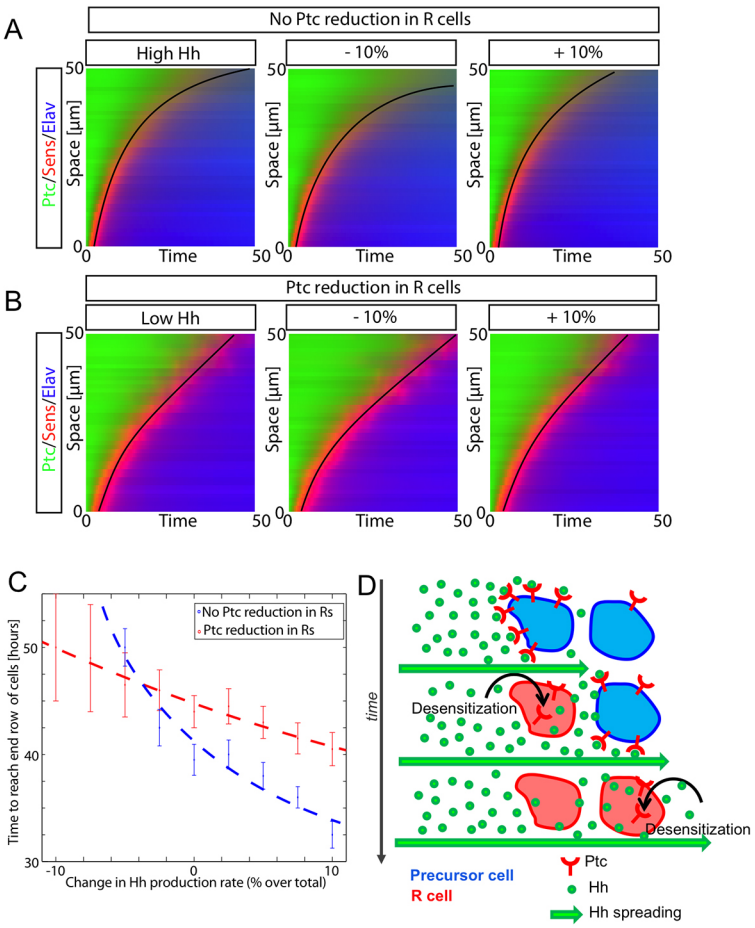

Fig. 5. Robustness in the dynamics of the wave against changes in Hh increases when Ptc feedback is present. (A,B) Space-time plots when Hh concentration is increased and decreased by 10% compared in the absence (A) or presence (B) of Ptc reduction in R cells. Colours represent the expression levels of Ptc (green), Sens (red) and Elav (blue). The solid line is used to represent the speed of the wave as a guide to the eye. The intensity of Hh in the left panel in A has been adjusted to facilitate comparison between A and B. (C) Changes in the dynamics of the wave due to changes in Hh concentration. The model with no Ptc reduction (blue dashed line) is more sensitive to changes in Hh concentration than the situation with Ptc reduction. Statistics performed using 30 independent simulations for each point. Bars indicate the s.d. of each measurement. (D) Schematic depiction of the model proposed. Hh spreading leads to Ptc upregulation and maximal signal initially closest to the source. As the cells differentiate, Ptc levels decrease, allowing farther extension of Hh spreading. By each cell dynamically responding to Hh, the ocellar primordium transforms a noisy non-linearly decaying signal into a differentiation wave of constant speed that is robust to signal noise. Source code for Hh signalling model available in the supplementary material under source code File 1.

same disc. Whereas in control discs (*ato1*$^{-/+}$) the relative levels of Ptc decrease with time (Fig. S6A,B), Ptc expression is maintained at levels comparable with those found in control discs before the onset of R differentiation, despite their having been exposed to Hh for the whole duration of the third larval stage (Fig. S6C). To test directly whether R differentiation was causing Ptc downregulation, we drove uniform and premature Sens expression to force ocellar cells to differentiate prematurely. As expected, after Sens overexpression, the ocellar region of *eyaL>Sens* larvae had an increased number of Elav-expressing cells relative to stage-matched controls. These cells also showed a concomitant loss of Ptc expression (Fig. S6F,G). To investigate *ptc* regulation further, we analysed *ptc* expression using a *ptc-Z* transcriptional reporter. Indeed, *ptc-Z* signal falls in Elav-expressing cells, suggesting that, as differentiation proceeds, *ptc* is repressed transcriptionally (Fig. S7). Therefore, in the ocelli, R differentiation is a major controller of Ptc dynamics.

One important aspect of ocellar differentiation is that, by the end of development, the number of R cells per ocellus is very consistent (the number of R cells of the adult posterior ocellus is 47.9; s.d.=0.7; n=5). However, we have noticed in static measurements of Hh:GFP that its signal is highly variable (Fig. S4). To test for robustness, we compared the output of the model with or without signal desensitization, varying Hh production rates by up to 10%. Although without desensitization the dynamics were far from linear and the time to differentiation termination varied widely, the model including reduced Ptc availability coupled with differentiation maintained linearity (i.e. constant differentiation speed) and showed low variability in time to termination, despite these variations in production rates (Fig. 5, Fig. S8). Therefore, our model predicts that, in addition to promoting a differentiation wave of constant speed, the R differentiation-induced Ptc desensitization results in increased developmental reliability.

Previous work had shown, in different developmental contexts, how a spatially static source of Hh/Shh coupled to its intracellular signalling network could generate spatial patterns of gene expression (reviewed in Briscoe and Thérond, 2013). In all these cases, the dynamics of Ptc expression were shown to be particularly important. For example, in the *Drosophila* epidermis, Hh is produced in a stripe per segment. Early, Hh spreads over the whole width of the segment and represses the target gene *Serrate* (*Ser*). Later, as Ptc upregulation sharpens the gradient, Ser becomes expressed in cells most distal to the Hh source, with Ser cells contributing a specific cell type in the dorsal epidermis. Interestingly, different segments exhibit different temporal dynamics (with some segments never showing Ser expression) (Gallet and Therond, 2005), suggesting that the Hh/Ptc dynamics may be subject to the control of segment-specific Hox genes. Another example is the patterning of the vertebrate neural tube along its dorso-ventral axis by Shh, which is expressed in the floor plate. Here, the upregulation of the receptor Ptc1 not only results in a change in the signalling profile across the tissue, but also causes a progressive cell-autonomous desensitization of the pathway, as increasing levels of unbound Ptc1 inhibit the signal transduction pathway (Dessaud et al., 2007). This desensitization may resemble the one we have described here. However, in the ocellar retina, the pathway becomes desensitized by a reduction of Ptc expression, which involves its transcriptional downregulation in photoreceptor cells.

In this article, we show that a spatially static Hh source can also be decoded as a linear ‘time arrow’ – a wave of differentiation of

Development (2019) 146, dev176933. doi:10.1242/dev.176933

photoreceptors with constant speed. This capacity requires a single change in the regulation of the Hh receptor Ptc. Two system-level properties are worth mentioning: First, the 'log-transform' of the signal of the gradient is an active process, in the sense that cells are not passive readers, but transform the signal dynamically through a reactive intracellular signalling network. Second, the mathematical transformation of the signal is an emerging property of the system: although the signalling changes operate at the single cell level, this transformation requires a number of cells coupled within a Hh gradient. Even though the pervasive use of Hh/Shh as a morphogen might be the result of evolutionary contingencies, an alternative explanation is that Hh and its signalling pathway, by acting on fields of cells, are flexible in the type of information outputs that cells generate when reading the gradient. It is conceivable that this flexibility would be a selective advantage that might have resulted in the Hh signalling pathway being redeployed once and again during evolution.

MATERIALS AND METHODS

Drosophila strains and genetic manipulations

Hh:GFP (BAC) was used to monitor the expression for Hh protein (Chen et al., 2017). *ato*^{1} is an *atonal* mutant allele (FlyBase) and *ato:GFP* has been described by Quan et al. (2016). GAL4/UAS crosses were set up at 29°C to maximize GAL4-driven expression, except when indicated. The *hh-GAL4, UAS-GFP:Hh* strain was used as reporter for Hh expression (Callejo et al., 2008). Elav-Gal4 (FlyBase) was used to drive UAS-*H2B-mCherry-P2A-eGFP-PH* line (Sánchez-Higueras and Hombría, 2016) in differentiated R cells, allowing the distinction between nuclei (mCherry) and cell membranes (eGFP) (experiment at 25°C). The FlyLight (Jenett et al., 2012) GAL4 line R20D09 from *eya* (herein referred to as EyaL-GAL4) was used to drive UAS transgenes specifically in the anterior and posterior ocellar competence domains (Fig. S2). UAS lines used were: UAS-nlsGFP (FlyBase), UAS-Ci-PKA (Methot and Basler, 2000) and UAS-GFP-*ptc*Δloop2 (UAS-*ptc*DN) (Briscoe et al., 2001). Larvae from crosses of *eyaL-GAL4* and UAS lines were raised at 29°C. GMRtdTom was used as a reporter of Glass to monitor the PR cells and membranes (Pappu et al., 2011). Quantification of the number of R cells over time was performed in the wild-type strain Oregon R at 25°C. To perturb the normal distribution of Hh, a GFP-tagged Hh (UAS-GFP:Hh; Torroja et al., 2004) was driven with the *wg2.11-GAL4* strain (*wg2.11-GAL4; UAS-GFP:Hh,* or 'wg>Hh'). wg2.11 is an enhancer of the *wg* gene that is expressed surrounding the ocellar region and overlapping the prospective interocellar region in the eye imaginal disc [described by Pereira et al. (2006) and see Results].

Immunofluorescence

Medium to late third instar larvae and pupae were dissected and fixed according to standard protocols. Immunostainings were performed as previously described (Bessa and Casares, 2005). We used the following primary antibodies: rabbit anti-GFP at 1:1000 (Molecular Probes), rat anti-RFP at 1:500 (Chromotek), rabbit anti-β-gal at 1:1000 (Cappel), mouse anti-Eya 10H6 at 1:400, rat anti-Elav 7EBA10 at 1:1000 and mouse anti-Ptc at 1:100 were from the Developmental Studies Hybridoma Bank. Aliquots of mouse anti-Sens at 1:250 were gifts from Andrew Jarman (University of Edinburgh, UK), Bassem Hassan (ICM, Paris, France), Rosa Barrio (Biogune, Leioa, Spain) and Xavier Franch (IBE-UPF, Barcelona, Spain), and rat anti-Ci 2A1 at 1:5 was a gift from Bob Holmgren (Northwestern University, Evanston, IL, USA). Imaging was carried out on Leica SP2, SPE or SP5 confocal microscope.

Measurement of the Hh:GFP signalling gradient dynamics

Eye discs from the BAC Hh:GFP strain were dissected from 96-130 h after egg laying (grown at 25°C) and stained simultaneously. Number of discs per experiment was 11 or more and one representative example is shown. Developmental stage was determined as number of ommatidial rows in the region of the compound eye. Imaging was carried out using a Leica SP5 confocal setup with the same settings. Lasers were warmed up beforehand for 1 h. Fluorescence intensity measurements were obtained with Fiji (Schindelin et al., 2012) by selecting a ROI across the ocellar complex. Then a Plot Profile was generated for the ROI and the quantitative data were obtained were processed in Excel.

R cell recruitment over-time

Medium-late third instar OR-R larvae and pupae were dissected and stained using anti-Elav antibodies to monitor the degree of differentiation from the stage 17 ommatidia to stage 27 ommatidia. The total number of samples quantified was 83 for both ocelli. Samples per time point ranged from five to 12. To analyse the correlation of the number of ocellar photoreceptors cells (Rs) and developmental time, as measured by the number of ommatidia rows in the compound eye, we performed an univariate linear regression, using the formula:

$$Y = \beta_0 + \beta_1 X + \varepsilon; \quad \varepsilon \sim N(0, \sigma^2),$$

where Y is the number of R cells, X is the number of ommatidial rows in the compound eye; β_0 is the intercept coefficient, β_1 is the number of ommatidial row coefficient, N is the number of data points and σ^2 is the variance and ε is the regression error. The model was estimated by the least squares method using the *lm()* function in Rsoftware and validated checking for normality, independence and homoscedasticity of residuals. The analysis shows a statistically significant linear dependence between PR cell number and developmental time, either when considering PR cell number of the anterior or the posterior ocelli individually or aggregating the data from both ocelli. Table 1 provides a summary of the statistical results of the linear regression.

Quantification of adult ocelli R cell number

Brain preparations, with the ocelli attached, were dissected from newly hatched (0-1 days) adults, stained with anti-Elav and counterstained with rhodamine-phalloidin (cell membranes) and DAPI (nuclei). Ocelli were imaged as *z*-stacks on an SPE Leica confocal setup and reconstructed using Imaris (Bitplane) for quantification.

Spatial statistics of Elav and Sens pattern under normal and perturbed Hh distribution

We imaged as confocal *z*-stacks ocellar regions stained for Sens and Elav from control (Oregon-R strain; *n*=19) or *wg2.11>GFP:Hh* (*n*=18), over the 18-23 ommatidia stage. Three cell states can be observed – (1) [Sens−, Elav+], (2) [Sens(weak), Elav(weak)] and (3) [Sens+, Elav−] – that correspond to differentiating photoreceptors, the transition between precursors and photoreceptors, and precursors, respectively. To obtain a bidimensional description of the distribution of these cells types in the tissue, we superimposed an orthogonal grid (ImageJ: Analyze>Tools>Grid) on a maximal projection of the *z*-stack sections comprising all Sens and Elav signals. The cell size of the grid is set to correspond approximately to the size of the nucleus of the cell, so that, in general, there is only one nucleus per cell of the grid. When a nucleus spans two or more cells in the grid, its position is allocated to the cell of the grid where most of the signal is. Then, a 1, 2 or 3 is assigned to each grid cell according to its Sens and Elav signal. A grid cell with no signal is assigned a '0'. The result is a two-dimensional matrix of positions of the three states per sample (Fig. S3).

Statistical analysis of Elav and Sens expression patterns

In order to test the departure from a random pattern of Sens and Elav expression, we defined two statistics: 'grouping' and 'polarity'. Importantly, the degree of polarization will tell whether the pattern is compatible with a

Table 1. R cell recruitment over time and parameters of the linear regression

	pOC	aOC	pOC+aOC
Coefficient estimated	2.8067	1.039	3.8386
Coefficient *P*-value	<2e-16	2.39E-15	<2e-16
R-squared	0.7722	0.5995	0.7794
Adjusted R-squared	0.7689	0.5937	0.7762
Model *P*-value	2.2E-16	2.391E-15	<2.2e-16

Development (2019) 146, dev176933. doi:10.1242/dev.176933

wave-like organization. For the analysis, each matrix comprising 1, 2 and 3 cell types (Elav+Sens−, Elav+Sens+ and Elav−Sens+, respectively) is split into two matrices, one in which 2 is identified as 1 and another in which 2 is identified as 3, because '2' is expression of 1 and 3 in the same cell. This allows a straightforward statistical analysis.

'Grouping' is defined as the departure from a random proportion of neighbours of a given type for each cell expressing Elav or Sens. For each cell *i*, the proportion of Elav- or Sens-expressing neighbours, p_i, is calculated as:

$$p_i = \frac{s_i}{n_i},$$

where s_i is the number of neighbours of a given type and n_i is the total number of neighbours [this number will depend on the position of the cell within the matrix, with cells in the centre with more neighbours (8) than those in the periphery]. Grouping is a global property of the ocellus, so the estimation of grouping for the whole ocellus could be reduce to count the number of Elav- or Sens-expressing cells relative to total cells in the neighbourhood:

$$P = \frac{\sum_i s_i}{\sum_i n_i}$$

However, this grouping is strictly dependent on the proportion of Elav or Sens in the ocellus, so in order to obtain an unbiased measure of grouping, the total proportion of cells expressing a factor needs to be subtracted from the proportion of this factor in the neighbourhood. As a correction of the statistic thus defined we actually consider the total proportion as:

$$\frac{S-1}{N-1}$$

Where S is the total number of cells expressing the factor in the ocellus and N the total number of cells in it. We have to subtract 1 from the numerator and denominator because each time we calculate the proportion of neighbours, we focus non-randomly on a cell expressing the factor (effectively we are 'removing' one case from the sample) so the proportion of success in the neighbourhood that can be expected in a random matrix would be lower than the actual proportion. Grouping of cells of the same type is the expressed as follows:

$$grouping(x) = P(x) - \frac{S_x - 1}{N-1},$$

where x is the expressed factor, Elav or Sens.

However, if we consider grouping of Elav around Sens or Sens around Elav, then making the previous correction is not needed because this time the expected proportion of success in the neighbourhood in a random matrix coincides with the total proportion in the ocellus. For the case of grouping of cells of one type (y) around a cell of the other type (x), the grouping would be defined as:

$$grouping(x,y) = P(x,y) - \frac{S_y}{N}$$

Where x is the expressed factor in a cell, and y is the other factor, expressed in the neighbourhood of the cell.

'Polarity' measures the ordered succession of cells states along a spatial axis. In our case, it is the 'proximodistal' axis with 'proximal' defined as the position closest to the endogenous Hh source. For each matrix and each factor, it is possible to define a dichotomous response variable Y that classifies a cell as expressing a factor, 1, or not, 0. So we can define a logistic regression model to predict the expression of this factor in a cell using column position X as a predictor:

$$Logit(Y)\tilde{\beta}_0 + \beta_1 X$$

The hypothesis for Elav is that its expression will be 'proximal', i.e. the left or first column, whereas Sens will be 'distal', i.e. the right or last column, so after the estimation of the model for each factor, we will use these models to predict the probability of finding ELAV in the first column and Senseless in the last one. The following expressions define them:

$$\text{If } \alpha = \text{Elav} \quad Polar(\alpha) = P(Y = 1|X = 1)$$

and

$$\text{If } \alpha = \text{Sens} \quad Polar(\alpha) = P(Y = 1|X = n),$$

where n is number of columns in the matrix and α is the factor used.

This probability has to be compared with the probability of finding expression of α at that column randomly or, what is the same, with no predictor used, which coincides again with the total proportion of the factor in the matrix. Polarity is then defined as follows:

$$Polarity(\alpha) = Polar(\alpha) - \frac{S_\alpha}{N}$$

Where S_α is the number of cells expressing the factor and N the number of cells in the matrix.

To carry out group comparison, for each matrix four measures of 'grouping' and two of 'polarity' were estimated:

$$grouping(Elav); grouping(Sens); grouping(Elav, Sens);$$
$$grouping(Sens, Elav) Polarity(Elav); \text{ and } Polarity(Sens).$$

Then they were calculated for every matrix and plotted (Fig. S3). In order to test for significant grouping differences between control and *wg>Hh*, a Welch's test for unequal variances was performed for each grouping variable:

$$\begin{cases} H_0 : \mu_1 = \mu_2 \\ H_1 : \mu_1 \neq \mu_2 \end{cases}.$$

As we aimed at testing whether there was a pattern of Elav and Sens expression, we had to check that they were not distributed randomly, so grouping should be larger than 0. Student's *t*-test for each grouping distribution and experimental group, control or *wg>Hh*, was performed:

$$\begin{cases} H_0 : \mu \leq 0 \\ H_1 : \mu > 0 \end{cases}.$$

The same hypothesis was posed and the same test performed for polarity, first to check whether these groups were significantly different from one another and then to check whether the polarity was larger than 0.

Statistics and data treatment were performed in R software. Data matrices were imported to R from.csv.

Adult cuticles dissections

The dorsal head capsules were dissected in PBS. Brain tissues and proboscis were removed from the samples. All the structures were incubated overnight in Hoyer's:Lactic Acid (1:1) solution at 80°C (Magri et al., 2018). Imaging was carried out on a Leica DM500B microscope with a Leica DFC490 digital camera. All images were processed with Fiji (Schindelin et al., 2012).

Modelling the Hh pathway in the *Drosophila* ocelli

Simulations were performed using an in-house computational script developed in Matlab (The Mathworks). This script is available as source code (Source code File 1). Equations are discretized in space and time using an Euler approach, with adimensional concentrations but dimensional variables in space and time. The model is based on a hybrid approach that combines partial differential equations (PDEs) solved in a continuous space and ordinary differential equations (ODEs) that are solved in a discrete space. The PDEs account for the diffusive extracellular signals, whereas the ODEs account of the intracellular reactions. Cells are simulated as two-dimensional regions in a hexagonal Voronoi diagram, with cell-to-cell variability introduced as gamma-distributed values for each of the kinetic constants of the reactions involved, with a standard deviation of 20% of the mean value.

The equations define a simplified representation of the Hh signalling pathway, illustrated in Fig. 3. Our model is based on the idea that the differentiation of photoreceptors regulated by Hh is a dynamic process,

Development (2019) 146, dev176933. doi:10.1242/dev.176933

owing to the fact that the amount of Hh that each cell in the tissue receives depends on time. To reduce free parameters and to try to obtain a simplified model that includes only the basic interactions that are required to reproduce the experimental observations, we have condensed all production and degradation rates in two constants (see Table 1). In addition, we have condensed all Hill coefficients in three constants. Free Hh degradation or Elav downregulation are not included in the model equations, as they are not relevant to the process studied by the model. The set of interactions that the model takes into account are outlined in the following paragraphs.

Diffusion of the Hedgehog (Hh) morphogen

Hh is secreted by producing cells in the intervening region between the anterior and posterior ocellar competent regions ('Hh source') and then disperses, generating a concentration gradient. The mechanism by which Hh disperses is not totally understood, and several studies propose that Hh travels through cytonemes (Gradilla and Guerrero, 2013) as an alternative to diffusion. Overall, the highly noisy spatiotemporal profile of Hh distribution in the ocellus (Fig. 4-Fig. S1) can be fitted with a second degree polynomial that decreases non-linearly when moving away from the Hh source. This fitting is used as a guide to the eye to illustrate how the profile of Hh changes in space and time, and to compare with the profiles derived from the model. Our model simplifies the details of Hh transport as two-dimensional diffusion. This approach successfully reproduces the experimental data of shape and dynamics of the Hh profile (see Fig. S3). The equation that governs Hh dynamics is:

$$\frac{\partial Hh(x,y,t)}{\partial t} = D \cdot \left(\frac{\partial^2 Hh(x,y,t)}{\partial x^2} + \frac{\partial^2 Hh(x,y,t)}{\partial y^2} \right) \quad (1)$$

As cells in the ocelli do not produce Hh, there is no production term in Eqn 1. Instead, our model approximates the Hh source as a continuous supply of Hh at one of the boundaries of the ocellus. The experimental data show that Hh expression by the Hh-producing cells, monitored by a Hh:GFP BAC, gradually decreases to 50% of its initial values during the period through which cell differentiation is taking place. This is introduced in our model as a continuous reduction in the Hh production rate at the production boundary to around 50% of its initial value. However, similar computational results are obtained if the Hh production rate is maintained constant (see Fig. S5). The modulation of Hh intensity is performed by setting a constant reduction of the rate of Hh expression in each iteration of the model, calculated to match a similar reduction in the rate of Hh at the source equivalent to the one observed experimentally.

Binding of Hh to its receptor Ptc

Hh binds to its receptor Ptc irreversibly to form a complex (*Ptc-Hh*) (Gallet and Therond, 2005; Incardona et al., 2002; Torroja et al., 2004), following the scheme:

$$Hh_i + Ptc_i \xrightarrow{k_{Hh}} Hh - Ptc_i, \quad (2)$$

where k_{Hh} corresponds to the affinity rate constant of the interaction. Hh_i corresponds to the amount of Hh that a given cell i is receiving, computed at each time step as the average value of Hh over the whole cell area of cell i. In this way, the continuous value of Hh computed in Eqn 1 is converted to a discrete value for each cell in the population Hh_i. This value is then used to compute the amount of Hh that binds to Ptc via Eqn 2, as an ODE that is solved for each cell in the hexagonal lattice:

$$\frac{\partial Hh_i(t)}{\partial t} = -k_{Hh} \cdot Ptc_i(t) \cdot Hh_i(t) \quad (3)$$

This ODE equation is then solved continuously in time but discretely in space, i.e. for each cell i in the population. The amount of Hh molecules consumed by each cell i in each particular position is the subtracted from the continuous spatial variable Hh in the corresponding position. The resulting Hh profile is then computed at the next time step using Eqn 1.

Expression of Ptc and binding to Hh

The amount of Hh that reaches a given cell in the population interacts with the free form of its receptor, Ptc. In the absence of Hh, free Ptc acts, indirectly through inhibition of the signal transducer Smo, as a repressor of Hh signalling target genes. This repression is set in the model as sigmoidal function of Ptc, with cooperativity m=3 (slightly higher or lower values of m also reproduce the experimental results). As one of Hh targets is Ptc itself, the sigmoidal repression is introduced in the equation corresponding to Ptc, forming a direct negative-feedback loop. In addition, a constant degradation of Ptc is introduced to ensure a dynamic equilibrium in its concentration. Taking this into account, the dynamics of Ptc is described by the following ODE:

$$\frac{\partial Ptc_i(t)}{\partial t} = \frac{\alpha_i \cdot A_i^m}{Ptc_i(t) + A_i^m} - k_{Hh} \cdot Ptc_i(t) \cdot Hh_i(t) - \frac{\beta_i \cdot Ptc_i(t) \cdot Elav_i^m(t)}{Elav_i^m(t) + C_i^m}, \quad (4)$$

where α and β corresponds to the rate constant for production and degradation. A corresponds to the half maximal concentration of the sigmoidal curve, and m sets the slope of the sigmoidal. The next term accounts for the binding of Ptc and Hh, following Eqn 2.

The second version of the model includes a reduction of available ('free') Ptc in terminally differentiated photoreceptors. This is simplified in the model by adding the last term in Eqn 4 in the form of a Hill function dependent on *Elav*, a marker of photoreceptor ('R') fate.

Expression of Senseless (Sens)

One of the relevant Hh signalling pathway targets (albeit likely indirect) is *senseless* (Sens), a zinc-finger transcription factor required for ocellar photoreceptor differentiation downstream of the proneural gene *atonal* (Nolo et al., 2000; Frankfort et al., 2001). Our model described the dynamics of expression of Sens by the following ODE:

$$\frac{\partial Sens_i(t)}{\partial t} = \frac{\alpha_i \cdot C_i^m}{Ptc_i^m(t) + C_i^m} \cdot \frac{A_i^m}{Elav_i^m(t) + A_i^m} - \beta_i \cdot Sens_i(t), \quad (5)$$

where the expression of *Sens* is mediated by simple direct repression by *Ptc*, where the half maximal concentration of the sigmoidal correspond to B. In addition, we have observed that, during ocellar differentiation, *Sens* expression is also lost in terminally differentiated photoreceptors. We represent this loss of *Sens* expression in the models as a direct repression by *Elav* in each cell i. To make this repression stronger than the repression by Ptc, the second term is elevated again to m.

Differentiation into a terminal photoreceptor cell

The events downstream of Sens that result in a terminally differentiated photoreceptor cells are also simplified in a single activation of the *elav* gene. Its expression is assumed as directly proportional to the amount of Sens. Therefore, the equation for the dynamics of Elav takes the form:

$$\frac{\partial Elav_i(t)}{\partial t} = \frac{\alpha_i \cdot Sens_i^m(t)}{Sens_i^m(t) + B_i^m} \quad (6)$$

Once the concentration of Elav reaches a given threshold value in a cell i, the model assumes an irreversible transition to a differentiated photoreceptor.

Acknowledgements

We thank T. Kornberg (UCSF), C. Sánchez-Higueras and J. C. G. Hombría (CABD), G. Struhl (Columbia University) and J. Culí (CBMSO) for fly strains; A. Jarman (University of Edinburgh), R. Holmgren (Northwestern University), B. Hassan (ICM), R. Barrio (Biogune), X. Franch (IBE-UPF) and I. Guerrero (CBMSO) for antibodies; and the CABD ALMI platform for imaging and image analysis support.

Competing interests

The authors declare no competing or financial interests.

Author contributions

Conceptualization: D.G.M., F.C.; Methodology: D.G.-M., T.N.; Software: D.G.M.; Formal analysis: T.N., D.G.M.; Investigation: D.G.-M., A.I., F.C.; Resources: P.S.P.;

Data curation: D.G.-M., F.C.; Writing - original draft: D.G.M., F.C.; Writing - review & editing: D.G.-M., T.N., D.G.M., F.C.; Visualization: D.G.-M., T.N., A.I., F.C.; Supervision: F.C.; Project administration: F.C.; Funding acquisition: D.G.M., F.C.

Funding
Research was funded through grants BFU2015-66040-P and MDM-2016-0687 (to F.C.) and BFU2014-53299-P (to D.G.M.) from the Ministerio de Ciencia, Innovación y Universidades (Spain).

Supplementary information
Supplementary information available online at
http://dev.biologists.org/lookup/doi/10.1242/dev.176933.supplemental

References

Aguilar-Hidalgo, D., Dominguez-Cejudo, M. A., Amore, G., Brockmann, A., Lemos, M. C., Cordoba, A. and Casares, F. (2013). A Hh-driven gene network controls specification, pattern and size of the Drosophila simple eyes. *Development* **140**, 82-92. doi:10.1242/dev.082172

Aguilar-Hidalgo, D., Becerra-Alonso, D., García-Morales, D. and Casares, F. (2016). Toward a study of gene regulatory constraints to morphological evolution of the Drosophila ocellar region. *Dev. Genes Evol.* **226**, 221-233. doi:10.1007/s00427-016-0541-8

Alexandre, C., Jacinto, A. and Ingham, P. W. (1996). Transcriptional activation of hedgehog target genes in Drosophila is mediated directly by the cubitus interruptus protein, a member of the GLI family of zinc finger DNA-binding proteins. *Genes Dev.* **10**, 2003-2013. doi:10.1101/gad.10.16.2003

Amin, A., Li, Y. and Finkelstein, R. (1999). Hedgehog activates the EGF receptor pathway during Drosophila head development. *Development* **126**, 2623-2630.

Aza-Blanc, P., Ramírez-Weber, F.-A., Laget, M.-P., Schwartz, C. and Kornberg, T. B. (1997). Proteolysis that is inhibited by hedgehog targets Cubitus interruptus protein to the nucleus and converts it to a repressor. *Cell* **89**, 1043-1053. doi:10.1016/S0092-8674(00)80292-5

Bessa, J. and Casares, F. (2005). Restricted teashirt expression confers eye-specific responsiveness to Dpp and Wg signals during eye specification in Drosophila. *Development* **132**, 5011-5020. doi:10.1242/dev.02082

Bilioni, A., Sánchez-Hernández, D., Callejo, A., Gradilla, A.-C., Ibáñez, C., Mollica, E., Carmen Rodríguez-Navas, M., Simon, E. and Guerrero, I. (2013). Balancing Hedgehog, a retention and release equilibrium given by Dally, Ihog, Boi and shifted/DmWif. *Dev. Biol.* **376**, 198-212. doi:10.1016/j.ydbio.2012.12.013

Blanco, J., Seimiya, M., Pauli, T., Reichert, H. and Gehring, W. J. (2009). Wingless and Hedgehog signaling pathways regulate orthodenticle and eyes absent during ocelli development in Drosophila. *Dev. Biol.* **329**, 104-115. doi:10.1016/j.ydbio.2009.02.027

Briscoe, J. and Thérond, P. P. (2013). The mechanisms of Hedgehog signalling and its roles in development and disease. *Nat. Rev. Mol. Cell Biol.* **14**, 416-429. doi:10.1038/nrm3598

Briscoe, J., Chen, Y., Jessell, T. M. and Struhl, G. (2001). A hedgehog-insensitive form of patched provides evidence for direct long-range morphogen activity of sonic hedgehog in the neural tube. *Mol. Cell* **7**, 1279-1291. doi:10.1016/S1097-2765(01)00271-4

Callejo, A., Culi, J. and Guerrero, I. (2008). Patched, the receptor of Hedgehog, is a lipoprotein receptor. *Proc. Natl. Acad. Sci. USA* **105**, 912-917. doi:10.1073/pnas.0705603105

Capdevila, J., Estrada, M. P., Sánchez-Herrero, E. and Guerrero, I. (1994). The Drosophila segment polarity gene patched interacts with decapentaplegic in wing development. *EMBO J.* **13**, 71-82. doi:10.1002/j.1460-2075.1994.tb06236.x

Casali, A. (2010). Self-induced patched receptor down-regulation modulates cell sensitivity to the hedgehog morphogen gradient. *Sci. Signal.* **3**, ra63. doi:10.1126/scisignal.2001059

Chamberlain, C. E., Jeong, J., Guo, C., Allen, B. L. and McMahon, A. P. (2008). Notochord-derived Shh concentrates in close association with the apically positioned basal body in neural target cells and forms a dynamic gradient during neural patterning. *Development* **135**, 1097-1106. doi:10.1242/dev.013086

Chen, Y. and Struhl, G. (1996). Dual roles for patched in sequestering and transducing Hedgehog. *Cell* **87**, 553-563. doi:10.1016/S0092-8674(00)81374-4

Chen, W., Huang, H., Hatori, R. and Kornberg, T. B. (2017). Essential basal cytonemes take up Hedgehog in the Drosophila wing imaginal disc. *Development* **144**, 3134-3144. doi:10.1242/dev.149856

Dessaud, E., Yang, L. L., Hill, K., Cox, B., Ulloa, F., Ribeiro, A., Mynett, A., Novitch, B. G. and Briscoe, J. (2007). Interpretation of the sonic hedgehog morphogen gradient by a temporal adaptation mechanism. *Nature* **450**, 717-720. doi:10.1038/nature06347

Frankfort, B. J., Nolo, R., Zhang, Z., Bellen, H. and Mardon, G. (2001). senseless repression of rough is required for R8 photoreceptor differentiation in the developing Drosophila eye. *Neuron* **32**, 403-414. doi:10.1016/S0896-6273(01)00480-9

Gallet, A. and Therond, P. P. (2005). Temporal modulation of the Hedgehog morphogen gradient by a patched-dependent targeting to lysosomal compartment. *Dev. Biol.* **277**, 51-62. doi:10.1016/j.ydbio.2004.09.005

Gradilla, A.-C. and Guerrero, I. (2013). Hedgehog on the move: a precise spatial control of Hedgehog dispersion shapes the gradient. *Curr. Opin. Genet. Dev.* **23**, 363-373. doi:10.1016/j.gde.2013.04.011

Heberlein, U., Wolff, T. and Rubin, G. M. (1993). The TGF beta homolog dpp and the segment polarity gene hedgehog are required for propagation of a morphogenetic wave in the Drosophila retina. *Cell* **75**, 913-926. doi:10.1016/0092-8674(93)90535-X

Hidalgo, A. and Ingham, P. (1990). Cell patterning in the Drosophila segment: spatial regulation of the segment polarity gene patched. *Development* **110**, 291-301.

Incardona, J. P., Gruenberg, J. and Roelink, H. (2002). Sonic hedgehog induces the segregation of patched and smoothened in endosomes. *Curr. Biol.* **12**, 983-995. doi:10.1016/S0960-9822(02)00895-3

Ingham, P. W., Nakano, Y. and Seger, C. (2011). Mechanisms and functions of Hedgehog signalling across the metazoa. *Nat. Rev. Genet.* **12**, 393-406. doi:10.1038/nrg2984

Jenett, A., Rubin, G. M., Ngo, T.-T. B., Shepherd, D., Murphy, C., Dionne, H., Pfeiffer, B. D., Cavallaro, A., Hall, D., Jeter, J. et al. (2012). A GAL4-driver line resource for Drosophila neurobiology. *Cell Rep.* **2**, 991-1001. doi:10.1016/j.celrep.2012.09.011

Ma, C., Zhou, Y., Beachy, P. A. and Moses, K. (1993). The segment polarity gene hedgehog is required for progression of the morphogenetic furrow in the developing Drosophila eye. *Cell* **75**, 927-938. doi:10.1016/0092-8674(93)90536-Y

Magri, M. S., Domínguez-Cejudo, M. A. and Casares, F. (2018). Wnt controls the medial-lateral subdivision of the Drosophila head. *Biol. Lett.* **14**, 20180258. doi:10.1098/rsbl.2018.0258

Methot, N. and Basler, K. (2000). Suppressor of fused opposes hedgehog signal transduction by impeding nuclear accumulation of the activator form of Cubitus interruptus. *Development* **127**, 4001-4010.

Nahmad, M. and Stathopoulos, A. (2009). Dynamic interpretation of hedgehog signaling in the Drosophila wing disc. *PLoS Biol.* **7**, e1000202. doi:10.1371/journal.pbio.1000202

Nakano, Y., Guerrero, I., Hidalgo, A., Taylor, A., Whittle, J. R. S. and Ingham, P. W. (1989). A protein with several possible membrane-spanning domains encoded by the Drosophila segment polarity gene patched. *Nature* **341**, 508-513. doi:10.1038/341508a0

Neumann, C. J. and Nuesslein-Volhard, C. (2000). Patterning of the zebrafish retina by a wave of sonic hedgehog activity. *Science* **289**, 2137-2139. doi:10.1126/science.289.5487.2137

Nolo, R., Abbott, L. A. and Bellen, H. J. (2000). Senseless, a Zn finger transcription factor, is necessary and sufficient for sensory organ development in Drosophila. *Cell* **102**, 349-362. doi:10.1016/S0092-8674(00)00040-4

Pappu, K. S., Morey, M., Nern, A., Spitzweck, B., Dickson, B. J. and Zipursky, S. L. (2011). Robo-3–mediated repulsive interactions guide R8 axons during Drosophila visual system development. *Proc. Natl. Acad. Sci. USA* **108**, 7571-7576. doi:10.1073/pnas.1103419108

Pereira, P. S., Pinho, S., Johnson, K., Couso, J. P. and Casares, F. (2006). A 3′ cis-regulatory region controls wingless expression in the Drosophila eye and leg primordia. *Dev. Dyn.* **235**, 225-234. doi:10.1002/dvdy.20606

Quan, X.-J., Yuan, L., Tiberi, L., Claeys, A., De Geest, N., Yan, J., van der Kant, R., Xie, W. R., Klisch, T. J., Shymkowitz, J. et al. (2016). Post-translational control of the temporal dynamics of transcription factor activity regulates neurogenesis. *Cell* **164**, 460-475. doi:10.1016/j.cell.2015.12.048

Royet, J. and Finkelstein, R. (1996). hedgehog, wingless and orthodenticle specify adult head development in Drosophila. *Development* **122**, 1849-1858.

Sánchez-Higueras, C. and Hombría, J. C.-G. (2016). Precise long-range migration results from short-range stepwise migration during ring gland organogenesis. *Dev. Biol.* **414**, 45-57. doi:10.1016/j.ydbio.2016.04.002

Schindelin, J., Arganda-Carreras, I., Frise, E., Kaynig, V., Longair, M., Pietzsch, T., Preibisch, S., Rueden, C., Saalfeld, S., Schmid, B. et al. (2012). Fiji: an open-source platform for biological-image analysis. *Nat. Methods* **9**, 676-682. doi:10.1038/nmeth.2019

Simon, E., Aguirre-Tamaral, A., Aguilar, G. and Guerrero, I. (2016). Perspectives on intra- and intercellular trafficking of Hedgehog for tissue patterning. *J. Dev. Biol.* **4**, 34. doi:10.3390/jdb4040034

Spratford, C. M. and Kumar, J. P. (2013). Extramacrochaetae imposes order on the Drosophila eye by refining the activity of the Hedgehog signaling gradient. *Development* **140**, 1994-2004. doi:10.1242/dev.088963

Torroja, C., Gorfinkiel, N. and Guerrero, I. (2004). Patched controls the Hedgehog gradient by endocytosis in a dynamin-dependent manner, but this internalization does not play a major role in signal transduction. *Development* **131**, 2395-2408. doi:10.1242/dev.01102

Vollmer, J., Fried, P., Sánchez-Aragón, M., Lopes, C. S., Casares, F. and Iber, D. (2016). A quantitative analysis of growth control in the Drosophila eye disc. *Development* **143**, 1482-1490. doi:10.1242/dev.129775

Wartlick, O., Jülicher, F. and Gonzalez-Gaitan, M. (2014). Growth control by a moving morphogen gradient during Drosophila eye development. *Development* **141**, 1884-1893. doi:10.1242/dev.105650

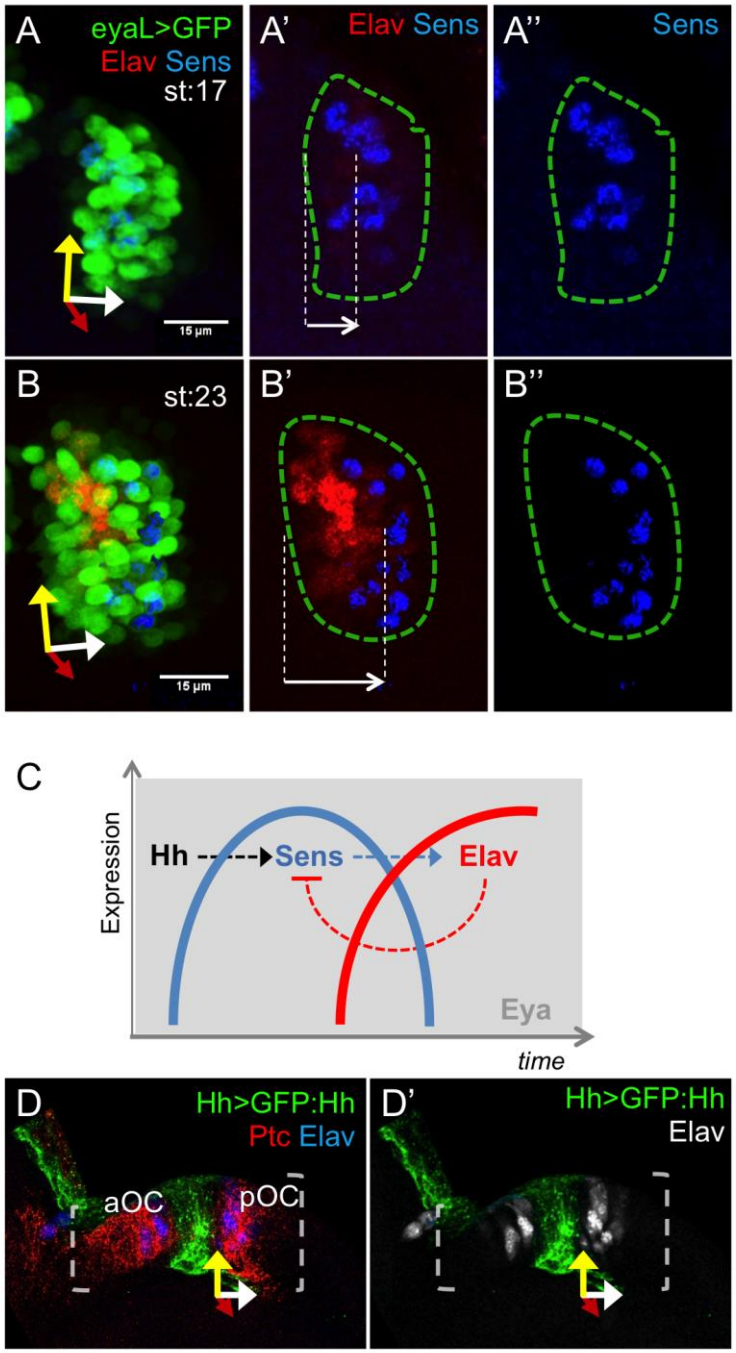

Figure S1. **R cells do not express Hh and differentiate following a *senseless-Elav* sequence**. (A,B) Sens and Elav mark the progress from precursors (Sens, red) to differentiating photoreceptors (Elav, blue). Confocal image of a posterior ocellar region of third instar stage 17 ommatidia (A) and 23 ommatidia (B) discs of an *eya>GFP* larvae. Eya (green) expression marks the ocellar competent region (outlined

in A'-A'' and B'-B''). At St17 Sens is expressed adjacent or close to the proximal border of the ocellus and no Elav R cells have yet differentiated. At St23, Elav R cells have differentiated and new Sens-positive cells are induced distal to them. The white arrows in A' and B' indicate the position of the Sens front relative to the Hh source. Axes as in Figure 1. (C) Schematic representation of the temporal changes in gene expression experienced by any cell in the ocellar complex. Competent cells (expressing Eya), upon receiving Hh signal, progress along their differentiation program, expressing Sens first, then Elav. The connecting links are dashed to indicate that the activations (arrow) or repression (flat end) are likely indirect. (D,D') Confocal image of an ocellar region (bracketed) from a *hh-Gal4>UAS-GFP:Hh* disc, stained for GFP, Ptc and Elav (D). (D') shows the GFP and Elav channels only. Elav-expressing R cells, which differentiate in a region of Hh signaling (i.e. Ptc-expressing), do not transcribe Hh.

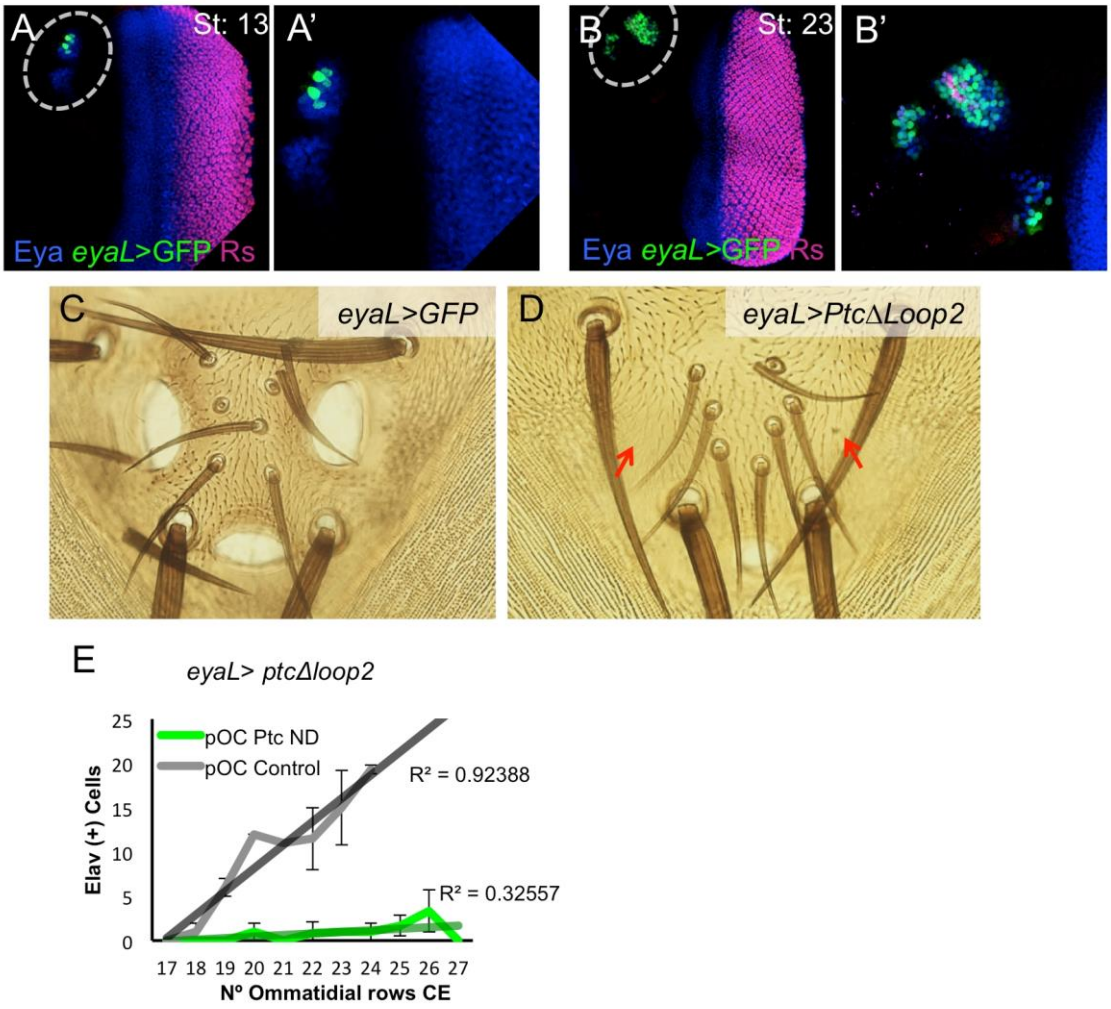

Figure S2. Driving a dominant-negative *Ptc* in the ocelli using the *eyaL-GAL4* blocks ocellar development. (A,B) Enhancer activity of the FlyLight R20D09 GAL4 driver line ("eyaL-GAL4") before (A: stage 13; A':close-up) and after (B: stage 23; B':close-up) R cell differentiation onset. Discs of eyaL-GAL4; UAS-GFP (*eyaL>GFP*) larvae were stained for Eya, GFP and Elav (R cells). Ocellar region is enclosed in the dashed oval. In (A), GFP signal is activated in the Eya-expressing ocellar domains. In later stages (B) GFP signal overlaps Eya. Therefore, EyaL-GAL4 drives expression in the ocellar *eya* domains exclusively. (C,D) Ocellar regions of adult flies. Control (C: *eyaL-GAL4; UAS-GFP*, "eyaL>GFP") and *eyaL-GAL4; UAS-ptcΔloop2* (D: "eyaL>ptcΔloop2"). PtcΔloop2 acts as a Hh-dominant negative protein (see Material and Methods and references). In *eyaL>ptcΔloop2* flies the ocelli are severely

reduced or absent (red arrows). (E) Dynamics of R cells differentiation in the posterior ocellus (pOC) (as Elav-expressing cells) in *eyaL>GFP* (“control”) and *eyal>ptcΔloop2* (“ptcDN”), with linear fits and R^2 values.

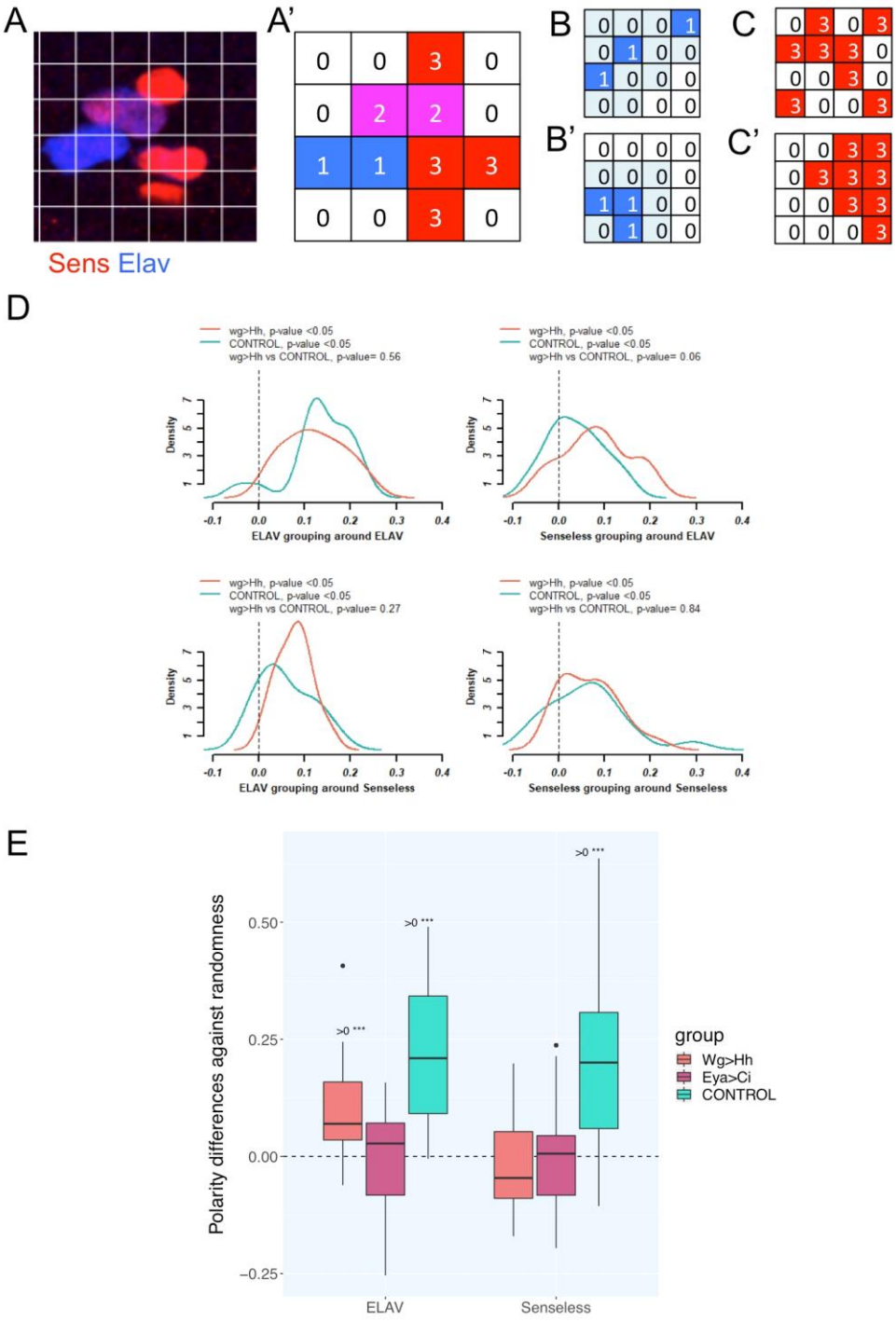

Figure S3. Statistical analysis of Sens/Elav pattern in control, *wg>Hh* and *eyaL>Ci-PKA* ocelli. (A) Image of a Sens and Elav staining with superimposed grid and its translation into a bidimensional matrix (A'), in which the three different states detected, Elav+Sens-, Elav(+)Sens(+) and Elav-Sens+ are coded as 1, 2 and 3, respectively. (B-C') Examples illustrating the two statistics used to analyze the pattern of Sens and Elav expression. (B,B') Example of "random" (B) and "grouped" (B') "1"

matrix. Neighbors are marked in light colors. From left to right and from top to bottom, the neighbor proportion is 0, 1/8 and 1/5, 0.1 on average for (B), and 2/5, 2/8 and 2/5, 0.4 on average for (B'). (C,C') Example of "non-polarized" (C) and "polarized" (C') "3" matrix. Polarity is calculated as the probability of finding a "3" in the last column, estimated using column number as predictor, minus the expected probability of success in the whole matrix (8/16). Polarity will be close to 0 for (C, "non-polarized") and significantly larger than 0 for (C', "polarized"). See methods and Results for further details. (D) Represents the departure from random grouping of different cell states ("order"). Both, control and *wg>Hh* patterns show significant ordered grouping for all four comparisons ($p<0.05$), although they do not differ significantly among them. "Density" refers to the density function, generated from the data histogram as a smoothened curve. (E) When the ordered distribution of Elav or Sens along the proximodistal axis ("polarity") is computed, the pattern in control ocelli is significantly polarized and much more so than in *wg>Hh* samples. This is also the case of *eyaL>Ci-PKA* samples. "0>***" refers to those groups in which their polarity were significantly higher than 0 ($p<0.05$). Only posterior ocelli were analyzed.

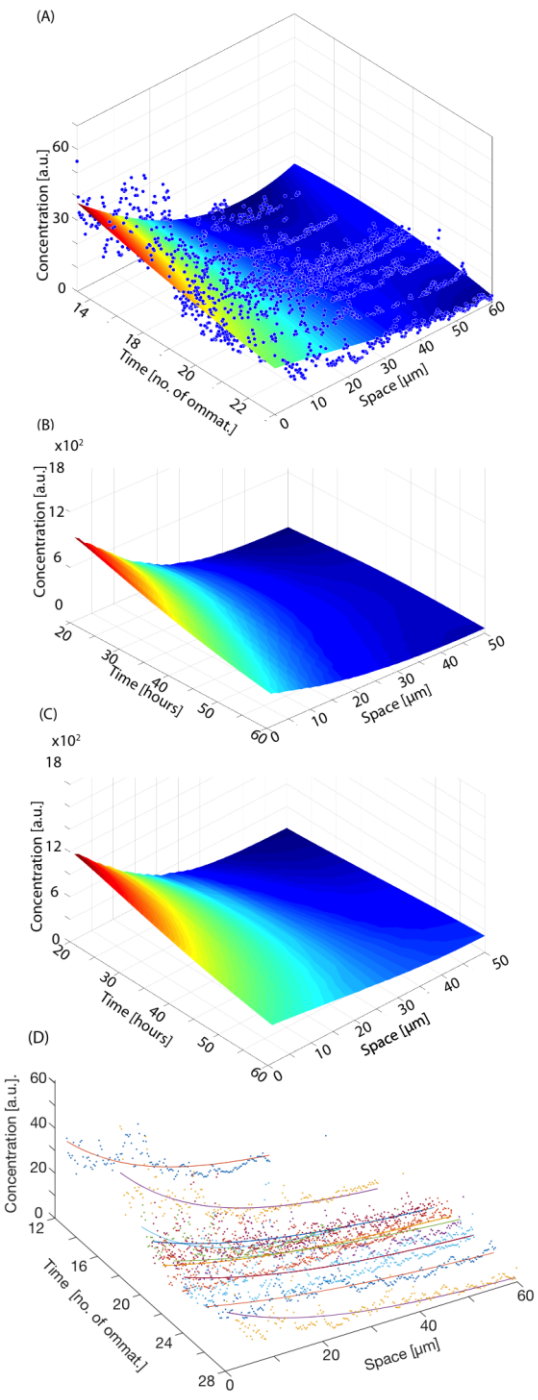

Figure S4. Hh gradient dynamics. (A) Plot of Hh:GFP signal (“concentration” in arbitrary units [a.u.]) as a function of time and space (in µm), obtained from fixed samples at specific developmental time points (as no. of ommatidia in the compound eye). Model parameters were constrained using this data. (B,C) Plots of Hh dynamics from the simulations, not

including (B) or including (C) the attenuation of Ptc expression in differentiating R cells. Note that in (C) (but not in (B)) the Hh gradient spreads farther with time, as observed in the measured profiles (A). (D) Exponential fitting (lines) of the spatial distribution of the Hh concentration profiles in (A).

Table S1. Values, units and sources of model parameters

Variable	value	Units	Source
Dimensions of Ocelus	55 x 55	μm^2	Experim. estimated
Number of cells in Ocelus	110	-	Experim. estimated
Number of cells in row	10	-	Experim. estimated
Number of rows	11	-	Experim. estimated
Total Time	50	hours	Experim. estimated
Rate of Hh expression 1	200		
High Rate of Hh expression	440		
k_{Hh}	0.002	1/hour	Value that best fits the experimental data
α	20	1/hour	fitted
β	10	1/hour	fitted
A	20	adimensional	fitted
B	1	adimensional	fitted
C	40		
m	3	adimensional	fitted
D	4	μm^2/hour	Value that best fits the experimental data.
Theshold for Elav	40		

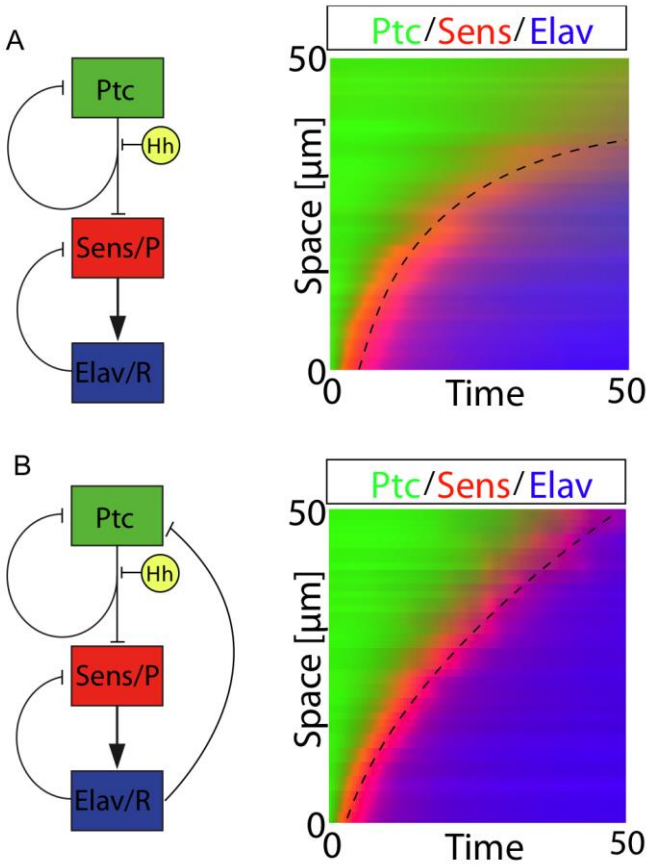

Figure S5. Differentiation dynamics and Ptc attenuation with a constant Hh production rate. Cartoon diagrams of the model for the Hh signaling pathway without considering (A) or considering (B) a negative feedback from Elav-expressing R cells to Ptc and its downstream effects (left), and corresponding spatio-temporal dynamics (right). In (A) R cells (blue) accumulate hyperbolically and do not reach the end of the competent region within the time frame of 50h. In (B) (with negative feedback, all other parameters being the same) R accumulation dynamics is close to linear and R differentiation reaches the end of the competent region. Simulations performed maintaining a constant Hh production rate.

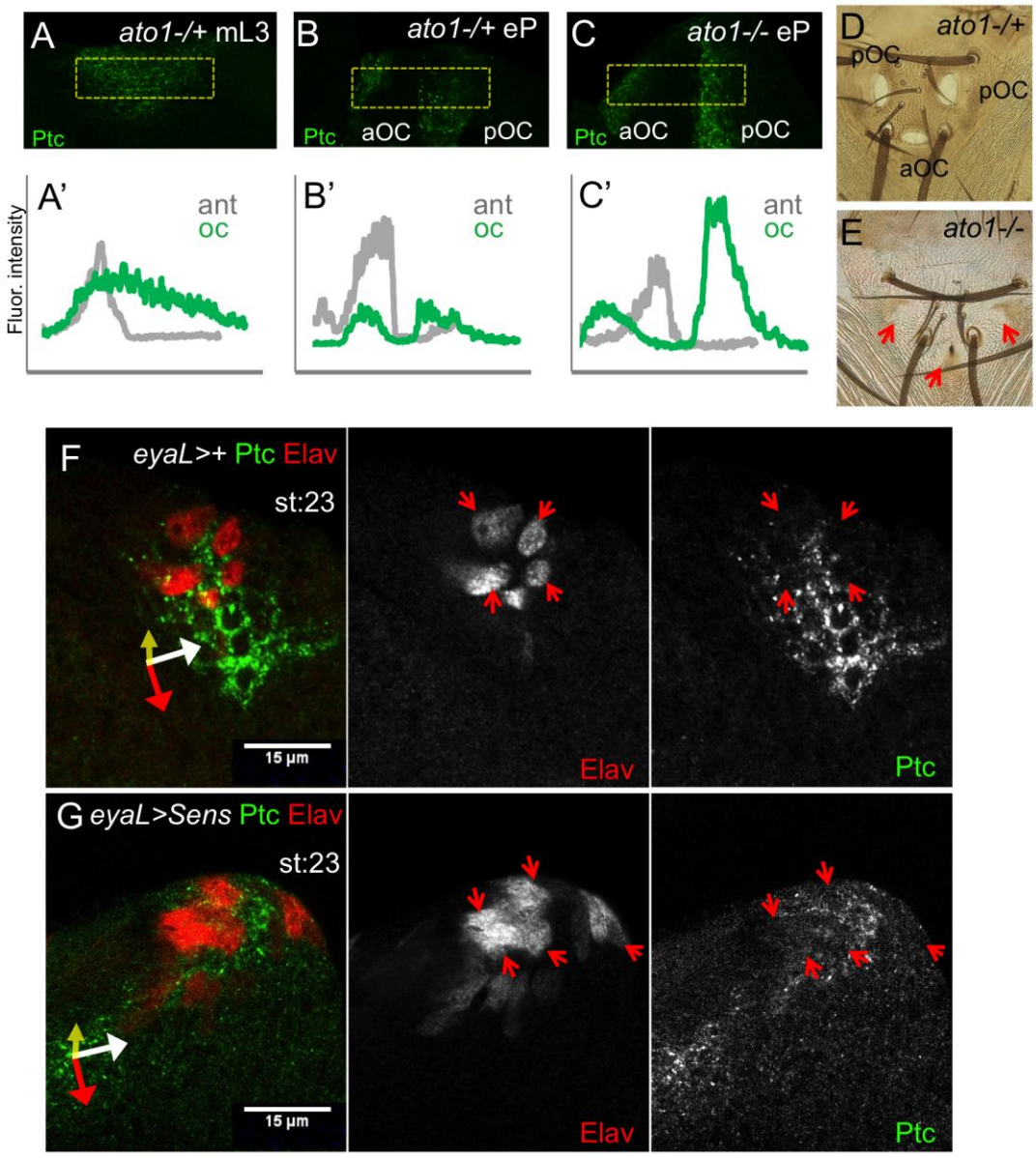

Figure S6. Ptc signal and R cell differentiation. (A-C) Ptc signal in the ocellar regions of mid L3 (mL3; A) and early pupa (eP; B) *ato1*+/- discs, and eP of an *ato1-/-* disc (C). (A'-C') Overlapped spatial expression profiles of Ptc signal in the ocellar regions ("oc", green) and in the antenna of the same disc ("ant", grey), this latter used as an internal normalization. In *ato1-/+* controls, the maximal ocellar Ptc signal is similar to that of the antenna (A'; n=6) in early discs but drops in later stages (early pupa: B', n=5). However, in late stage *ato1-/-* the Ptc signal ratio remains high (C'; n=6). Posterior and anterior ocelli (pOC and aOC) are marked in (B,C). In (A) the split

of the Ptc domain in the two ocellar primordia has not yet occurred. (D,E) Adult ocellar complexes of *ato1+/- and ato1-/-* flies. In homozygous *ato1* individuals ocelli fail to develop. (F,G) Control (F: *eyaL*>+) and Sens-expressing (G: *eyaL*>*Sens*) pOC at st:23 stained for Elav and Ptc. In *eyaL*>*Sens* there is an increase in the number of Elav cells. Ptc signal is reduced in all Elav cells and, as a consequence, in *eyaL*>*Sens* Ptc levels are globally reduced also. Red arrows point to Elav cells.

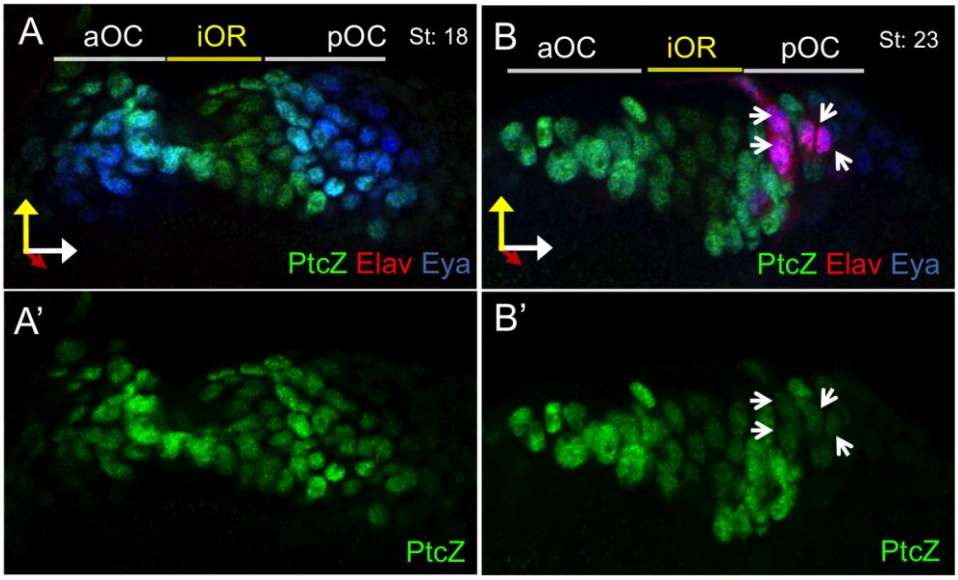

Figure S7. Expression of a *ptc* transcriptional reporter (ptc-Z) is down regulated in differentiating photoreceptors. Ocellar complex region of *ptc-Z* discs stained for β-galactosidase (PtcZ), Elav and Eya (A,B). PtcZ channel alone is shown in (A',B'). St 18 ocellar complex region, prior to the initiation of R cell differentiation. (B,B') St 23 ocellar complex region. Arrows point to Elav-expressing R cells. The anterior (aOC) and posterior (pOC) ocellar retinas as well as the interocellar region (iOR) are marked. PtcZ signal in the iOR is detected, although weak, likely due to β-galactosidase perdurance.

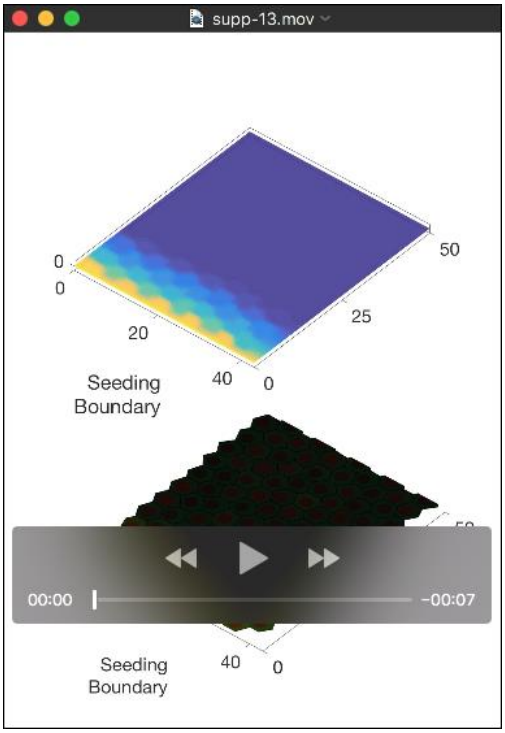

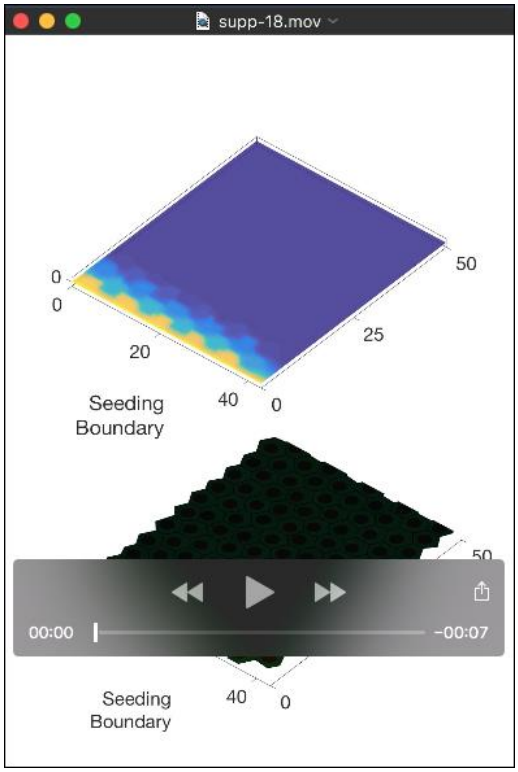

Movies 1 and 2. Time-lapse movies of the simulation without (Movie 1) and with (Movie 2) Ptc negative feedback regulation.

Upper panel shown the concentration of Hh across the domain. Lower panel shows the cellular concentration of Ptc (green), Sens (red) and Elav (blue). Despite the

variable response to Hh due to cell variability, a wave in photoreceptor differentiation (blue cells) can be observed as traveling away from the Hh source. The first movie (no Ptc downregulation) shows that the wave velocity diminishes and stops before reaching the end of the domain. The Hh gradient does not flatten. The second movie includes Ptc negative feedback, and shows how the differentiation wave moves at constant speed and reaches the end of the domain. The Hh gradient flattens.

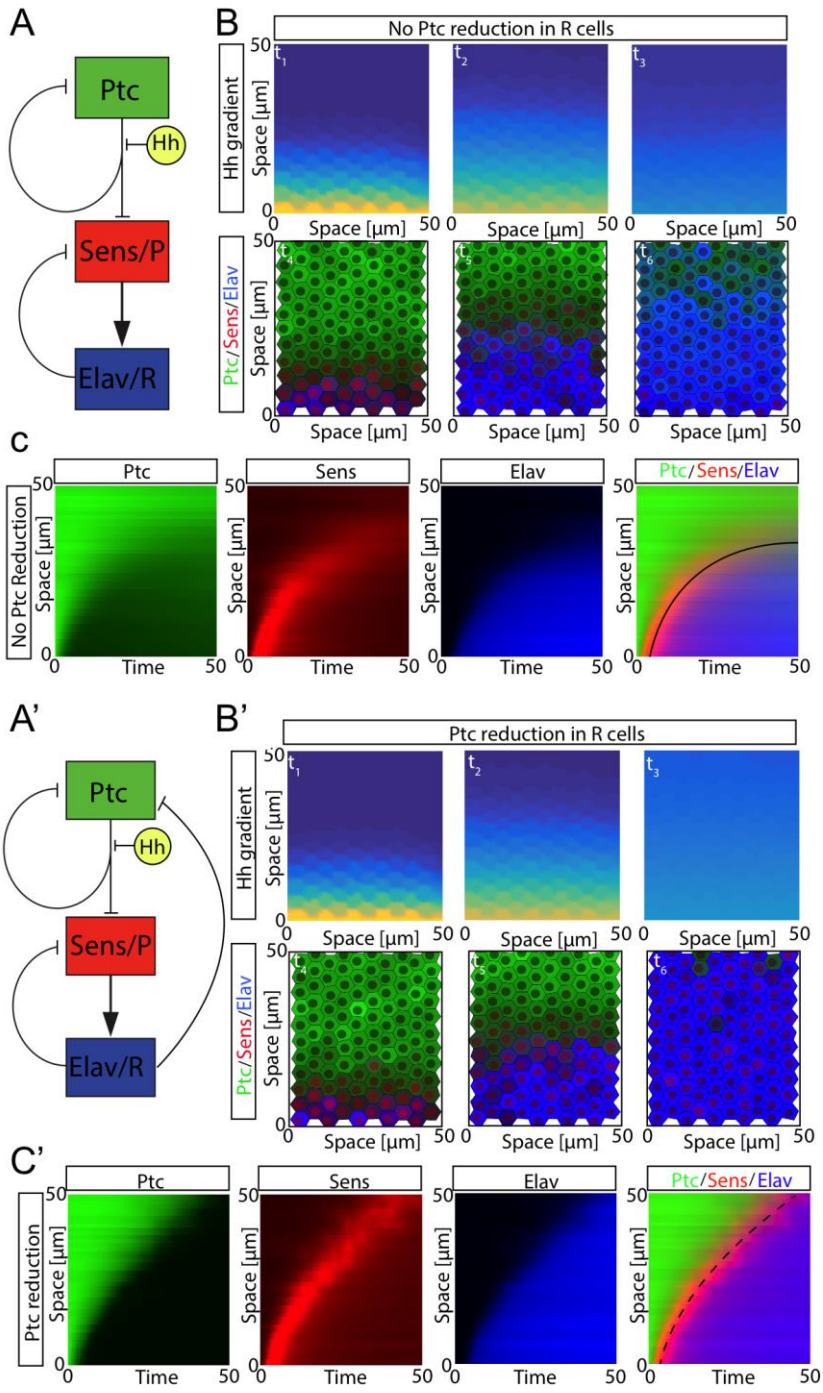

Figure S8. Dynamics of Hh signaling in response to its gradient. (A,A') Shape of the interactions taken into account in the model. (B,B') Snapshots of the simulation at different times. Images above depict the Hh profile, while the bottom images represent the cell differentiation state. Red: Sens cells; Blue: Elav R cells; Green: free Ptc (See supp. videos 1 and 2). (C,C') Space-time plots of free Ptc (green),

Sens (red) and Elav (blue) and superposition of the three across the ocellus. The black lines (solid in (C) and dashed in (C')) are used as a guide to the eye to show the speed of the differentiation wave.

The source code file can be downloaded here